Modal analysis of a multi-blade system undergoing rotational motion [†]

Ha Seong Lim and Hong Hee Yoo[*]

Department of Mechanical Engineering, Hanyang University, Seoul, 133-791, Korea

---

Abstract

A modeling method for the modal analysis of a multi-blade system undergoing rotational motion is presented in this paper. Blades are assumed as cantilever beams and the coupling stiffness which originates from the shroud flexibility is considered for the modeling. To obtain general conclusions from the numerical results, the equations of motion are transformed into a dimensionless form. Dimensionless parameters related to the angular speed, the hub radius, and the coupling stiffness are identified and the effects of the parameters on the modal characteristics of the system are investigated. It is shown that the coupling stiffness especially plays an important role to change the modal characteristics of the system. The range of critical angular speed is also obtained through the numerical analysis.

Keywords: Modal analysis; Multi-blade; Rotational motion; Coupling stiffness; Dimensionless parameter; Critical angular speed

---

1. Introduction

Rotating multi-blade systems can be found in several engineering examples such as turbine generators, turbo engines, turbo fans, and rotorcraft wings. These structures are comprised of several blades which are attached to a hub (or a disk) and often connected through shrouds. Since the shrouds possess flexibility, they create stiffness coupling effects between blades. The stiffness coupling effects along with the angular motion influence the modal characteristics of the system significantly. To design such structures, therefore, the effects of the stiffness coupling as well as the angular motion of the multi-blade system need to be considered to estimate their modal characteristics accurately.

Study on the natural frequency variation of a rotating flexible structure originated from the work by Southwell and Gough [1]. They developed an analytical model (often called the Southwell equation) to calculate the natural frequencies of a rotating beam.

Later, Schilhansl [2] derived the equations of motion for rotating cantilever beams and obtained more accurate coefficients for the Southwell equation based on the Ritz method. Since early 1970s, the astonishing progress of computing technologies has enabled one to calculate the modal characteristics of the rotating beam with several numerical methods. A large amount of literature relating to this subject can be found (see, for instance, Refs. [3, 4]). Recently, a dynamic modeling method employing a hybrid set of deformation variables was introduced (see Refs. [5, 6]). Linear equations of motion can be derived with the modeling method. Even if the equations of motion are linear they can capture the stiffness variation effects induced by the rotational motion. The equations also include the coupling effect between stretching and bending motions. So the effect of the coupling effect on the modal characteristics of the rotating beam could be successfully investigated with the modeling method (see Ref. [7]).

In most of the studies mentioned in the previous paragraph, the modal characteristics of a single blade were only investigated. The study on the modal characteristics of a multi-blade system was presented only in a few papers (see Refs. [8, 9]). To obtain the modal

---

characteristics of a multi-blade system, the finite element method can be employed effectively. However, if the finite element method is employed the equation size becomes huge for the multi-blade system. Such a huge size model is not proper for the purpose of system design. Furthermore, a parameter study for design cannot be done with the finite element model. Therefore, a simplified model in which blades were idealized as rigid pendulums having a discrete torsional spring was employed for designs in those previous studies. The simplified model was employed in Ref. [8] and the FE model was employed in Ref. [9]. However, these models are too simple or too complex so that they are not proper for the design of a rotating blade system.

The purpose of the present study is to develop a linear dynamic model to analyze the modal characteristics of rotating multi-blade systems and to investigate the effects of some important parameters on the modal characteristics of the system using the model. To achieve the purpose, the equations of motion are derived based on the hybrid deformation variable modeling method (see Ref. [6]) and they are transformed into a dimensionless form in which some dimensionless parameters related to the angular speed, the hub radius, the shroud coupling stiffness, and the attachment location of the shroud spring are identified. The effect of the number of blades on the modal characteristics of the system is also investigated with the proposed model.

2. Equations of motion

In this section, equations of motion of a rotating multi-blade system are derived based on the hybrid deformation variable modeling method introduced in reference [6] where only a single blade was considered. To focus on the main issue of the present study (the effects of the coupling stiffness between multiple blades ad the angular motion), the following assumptions are made in this study. All the blades are assumed to be identical and only in-plane deformation occurs. Blades are assumed to have a slender shape and isotropic material property. So the stretching and the bending deformations are only considered, while the shear, the rotary inertia, the eccentricity, and the warping effects are neglected.

Fig. 1 shows the configuration of a multi-blade system. The blades are attached to a rigid hub A having radius r. $\hat{a}_1$ and $\hat{a}_2$ represent unit vectors
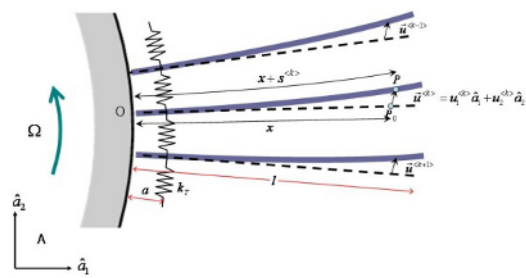

Fig. 1. Configuration of a multi-blade system.

attached to the rigid hub; x denotes the length from the point O to the point P_0 (the generic point of the beam before deformation occurs); k denotes the coupling stiffness of the shroud spring; a denotes the attachment position of the spring; $\vec{u}^{<k>}$ denotes the elastic deformation vector of n-th beam; and $s^{<k>}$ denotes the stretch of the beam. Employing the Rayleigh-Ritz assumed mode method, a hybrid set of variables $s^{<k>}$ and $u_2^{<k>}$ can be approximated as follows:

$$s^{<k>}(x,t) = \sum_{i=1}^{\mu_1} \phi_{1i}(x) q_{1i}^{<k>}(t) \tag{1}$$

$$u_2^{<k>}(x,t) = \sum_{i=1}^{\mu_2} \phi_{2i}(x) q_{2i}^{<k>}(t) \tag{2}$$

where ϕ_{1i} and ϕ_{2i} denote the longitudinal and the bending mode functions; $q_{1i}^{<k>}$ and $q_{2i}^{<k>}$ denote the generalized coordinates for the two mode functions respectively; and μ_1 and μ_2 denote the numbers of the generalized coordinates. When the rigid hub rotates with an angular speed Ω, the angular velocity of the rigid hub A and the velocity of the generic point P (the generic point of the beam after deformation occurs) can be obtained as follows.

$$\bar{\omega}^A = \Omega\hat{a}_3 \tag{3}$$

$$\vec{v}^P = \left[\dot{u}_1^{<k>} - \Omega u_2^{<k>}\right]\hat{a}_1 + \left[r\Omega + \dot{u}_2^{<k>} + \Omega(x + u_1^{<k>})\right]\hat{a}_2 \tag{4}$$

where $\dot{u}_1^{<k>}$ need to be expressed with respect to $\dot{s}^{<k>}$ and $\dot{u}_2^{<k>}$. The following geometric relation (see Ref. [6] in detail) can be used for the purpose.

$$\dot{s}^{<k>} = \dot{u}_1^{<k>} + \int_0^x \left(\frac{\partial u_2^{<k>}}{\partial \sigma}\right)\left(\frac{\partial \dot{u}_2^{<k>}}{\partial \sigma}\right) d\sigma \tag{5}$$

If the Kane's method (see Ref. [10]) is employed, the equations of motion for the system can be derived with the following equation.

$$\int_0^l \rho \left(\frac{\partial \vec{v}^P}{\partial \dot{q}_i} \right) \cdot \frac{d\vec{v}^P}{dt} dx + \frac{\partial U^{<k>}}{\partial q_i} = 0 \tag{6}$$

where l denotes the length of the beam, ρ denotes the mass per unit length of the beam, and q_i denotes the generalized coordinate. In Eq. (6), $U^{<k>}$ denotes the strain energy of the beam which can be given as

$$U^{<k>} = \frac{1}{2} \int_0^l \left[EA \left(\frac{\partial s^{<k>}}{\partial x} \right)^2 dx + EI \left(\frac{\partial^2 u_2^{<k>}}{\partial x^2} \right)^2 dx \right]$$
$$+ \frac{1}{2} k_T \left[u_2^{<k>}(a) - u_2^{<k-1>}(a) \right]^2 \tag{7}$$
$$+ \frac{1}{2} k_T \left[u_2^{<k+1>}(a) - u_2^{<k>}(a) \right]^2$$

where E, A and I represent Young's modulus, the cross-section area and the second area moment of inertia of the beam, respectively. Employing Eqs. (1-7), the equations of motion of the k-th beam can be derived as follows:

$$\sum_{j=1}^{\mu_1} \left[m_{ij}^{11} \ddot{q}_{1j}^{<k>} - \Omega^2 m_{ij}^{11} q_{1j}^{<k>} + k_{ij}^S q_{1j}^{<k>} \right]$$
$$- \sum_{j=1}^{\mu_2} \left[2\Omega m_{ij}^{12} \dot{q}_{2j}^{<k>} + \dot{\Omega} m_{ij}^{12} q_{2j}^{<k>} \right]$$
$$= r\Omega^2 P_{1i} + \Omega^2 Q_{1i} \qquad (i = 1, \cdots, \mu_1) \tag{8}$$

$$\sum_{j=1}^{\mu_2} \left[m_{ij}^{22} \ddot{q}_{2j}^{<k>} + \left\{ k_{ij}^B + \Omega^2 (k_{ij}^{GA} + k_{ij}^{GB} - m_{ij}^{22}) \right\} q_{2j}^{<k>} \right.$$
$$\left. - \left(k_{ij}^C q_{2j}^{<k-1>} - 2k_{ij}^C q_{2j}^{<n>} + k_{ij}^C q_{2j}^{<k+1>} \right) \right]$$
$$+ \sum_{j=1}^{\mu_1} \left[2\Omega m_{ij}^{21} \dot{q}_{1j}^{<k>} + \dot{\Omega} m_{ij}^{21} q_{1j}^{<k>} \right]$$
$$= -r\dot{\Omega} P_{2i} - \dot{\Omega} Q_{2i} \qquad (i = 1, \cdots, \mu_2) \tag{9}$$

where

$$m_{ij}^{ab} = \int_0^l \rho \phi_{ai}(x)\phi_{bj}(x)dx$$
$$k_{ij}^S = \int_0^l EA\phi_{1i,x}(x)\phi_{1j,x}(x)dx$$
$$k_{ij}^B = \int_0^l EI_{zz} \varphi_{2i,xx}(x)\varphi_{2j,xx}(x)dx$$
$$k_{ij}^{GA} = \int_0^l \rho r(l-x)\phi_{2i,x}(x)\phi_{2j,x}(x)dx \tag{10}$$

$$k_{ij}^{GB} = \int_0^l \frac{\rho}{2}\left(l^2 - x^2\right)\phi_{2i,x}(x)\phi_{2j,x}(x)dx$$
$$k_{ij}^C = k_T \phi_{2i}(a)\phi_{2j}(a)$$
$$P_{ai} = \int_0^l \rho\phi_{ai}(x)dx \tag{6}$$
$$Q_{ai} = \int_0^l \rho x\phi_{ai}(x)dx$$

In the above expressions, $\phi_{1i,x}$ and $\phi_{2i,x}$ indicate the differentiation of the symbols ϕ_{1i} and ϕ_{2i} with respect to x and $\phi_{2i,xx}$ indicates the double differentiation of the symbol.

For slender beams, the extensional natural frequencies are much higher than the bending natural frequencies. Therefore, the coupling effect between the extensional motion and the bending motion can be ignored without losing the accuracy of the analysis. So the following equation (by neglecting the coupling terms and the non-homogeneous terms from Eq. (9)) will be employed for the modal analysis.

$$\sum_{j=1}^{\mu_2} \left[m_{ij}^{22} \ddot{q}_{2j}^{<k>} + \left\{ k_{ij}^B + \Omega^2 \left(k_{ij}^{GA} + k_{ij}^{GB} - m_{ij}^{22} \right) \right\} q_{2j}^{<k>} \right.$$
$$\left. - \left(k_{ij}^C q_{2j}^{<k-1>} - 2k_{ij}^C q_{2j}^{<k>} + k_{ij}^C q_{2j}^{<k+1>} \right) \right] = 0 \tag{11}$$

It is useful to write the equations of motion in a dimensionless form. To achieve this, the following dimensionless variables are employed:

$$\tau = \frac{t}{T}, \qquad \xi = \frac{x}{l}, \qquad \theta_i = \frac{q_{2i}}{l} \tag{12}$$

where

$$T = \sqrt{\frac{\rho l^4}{EI}}$$

By employing the above dimensionless variables in Eq. (12), Eq. (11) can be rewritten as follows:

$$\sum_{j=1}^{\mu} \left[M_{ij} \ddot{\theta}_j^{<k>} + \left\{ K_{ij}^B + \gamma^2 \left(K_{ij}^{GA} + K_{ij}^{GB} - M_{ij} \right) \right\} \theta_j^{<k>} \right.$$
$$\left. - \left(K_{ij}^C \theta_j^{<k-1>} - 2K_{ij}^C \theta_j^{<k>} + K_{ij}^C \theta_j^{<k+1>} \right) \right] = 0 \tag{13}$$

where $\ddot{\theta}_j^{<k>}$ denotes the double differentiation of $\theta_j^{<k>}$ with respect to τ, γ denotes the dimensionless angular speed which can be obtained by the angular speed Ω multiplied by T and

$$M_{ij} = \int_0^1 \varphi_i(\xi)\varphi_j(\xi)d\xi$$

$$K_{ij}^B = \int_0^1 \varphi_{i,\xi\xi}(\xi)\varphi_{j,\xi\xi}(\xi)d\xi$$

$$K_{ij}^{GA} = \delta\int_0^1 (1-\xi)\varphi_{i,\xi}(\xi)\varphi_{j,\xi}(\xi)d\xi \qquad (14)$$

$$K_{ij}^{GB} = \frac{1}{2}\int_0^1 (1-\xi^2)\varphi_{i,\xi}(\xi)\varphi_{j,\xi}(\xi)d\xi$$

$$K_{ij}^C = \beta\varphi_i(\alpha)\varphi_j(\alpha)$$

In the above expressions, φ_j is a function of ξ which has the same functional value as $\phi_j(x)$. Three more dimensionless parameters are employed in the above expressions and they are defined as follows:

$$\alpha = \frac{a}{l}, \qquad \beta \equiv \frac{k_T l^3}{EI}, \qquad \delta \equiv \frac{r}{l} \qquad (15)$$

Now by assembling n sets of the equations written in Eq. (13), the total equations of motion for a multi-blade system can be written as follows:

$$\left[\overline{M}\right]\{\ddot{\theta}\} + \left[\overline{K}\right]\{\theta\} = \{0\} \qquad (16)$$

where

$$\left[\overline{M}\right] = \begin{bmatrix} [M] & 0 & \cdots & 0 & 0 \\ 0 & [M] & & & \vdots \\ \vdots & & \ddots & & 0 \\ & & & [M] & \\ 0 & 0 & \cdots & 0 & [M] \end{bmatrix}$$

$$\left[\overline{K}\right] = \begin{bmatrix} [K]+[K^C] & -[K^C] & \cdots & & 0 \\ -[K^C] & [K]+2[K^C] & \cdots & & \\ \vdots & & \ddots & & \vdots \\ & & & [K]+2[K^C] & -[K^C] \\ 0 & & \cdots & -[K^C] & [K]+[K^C] \end{bmatrix}$$

where

$$K_{ij} = K_{ij}^B + \gamma^2\left(K_{ij}^{GA} + K_{ij}^{GB} - M_{ij}\right)$$

For the modal analysis of the system, a column matrix $\{\theta\}$ can be expressed as follows:

$$\{\theta\} = e^{j\omega\tau}\{\eta\} \qquad (17)$$

where, ω denotes the dimensionless natural frequency and $\{\eta\}$ denotes the mode vectors. Substi-

tuting Eq. (17) into Eq. (16), one can obtain the following equation:

$$\omega^2\left[\overline{M}\right]\{\eta\} = \left[\overline{K}\right]\{\eta\} \qquad (18)$$

The modal analysis of a multi-blade system will be done by using Eq. (18) in the next section.

3. Numerical results

To obtain accurate numerical results, five assumed modes (which are the bending eigenmode functions of a cantilever beam) are employed for each beam to obtain the natural frequencies and the corresponding mode shapes.

Numerical results obtained by using the present modeling method are compared to those in [9], which provides some analytical solutions. The lowest nine natural frequencies of a 3-beam system are shown in Table 1 for which $\alpha = 0.1, \beta = 10, \gamma = 0, \delta = 0$ are employed. It is found that the results obtained by the present modeling method are almost identical to those of [9].

Fig. 2 shows the lowest eight dimensionless natural frequencies of 4-beam system versus the dimensionless angular speed. The parameters employed for the analysis are $\alpha = 0.1$, $\beta = 10$ and $\delta = 0.1$. As shown in the figure, there exist two groups of natural frequencies. The first group includes the lowest four natural frequencies and the second group includes the next four natural frequencies. Since the coupling stiffness β is not large enough, the natural frequencies in each group are almost identical. The figure also shows that the natural frequencies increase as the angular speed increases.

Fig. 3 shows the corresponding eight mode shapes of the 4-beam system. As shown in the figure, the
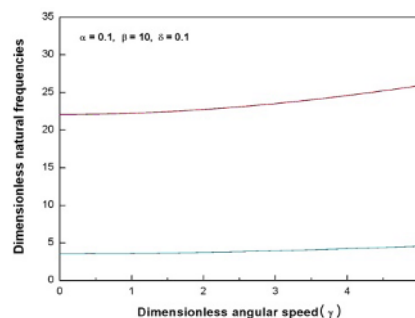

Fig. 2. Lowest 8 natural frequencies of the 4 beam system versus the angular speed.

Table 1. Comparison of the natural frequencies ($\alpha = 0.1$, $\beta = 10$, $\gamma = 0$).

Frequencies		Present	Ref. (9)
First Set	1st.	3.517	3.517
	2nd.	3.519	3.519
	3rd.	3.521	3.521
Second Set	4th.	22.04	22.04
	5th.	22.05	22.05
	6th.	22.06	22.06
Third Set	7th.	61.71	61.71
	8th.	61.73	61.73
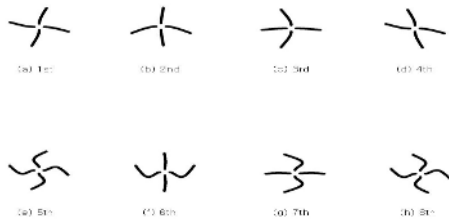
Fig. 3. Lowest 8 mode shapes of the 4-beam system.

(a) $\alpha = 0.5$

(b) $\alpha = 1.0$

Fig. 4. Lowest 8 natural frequencies versus the angular speed for different values of α.

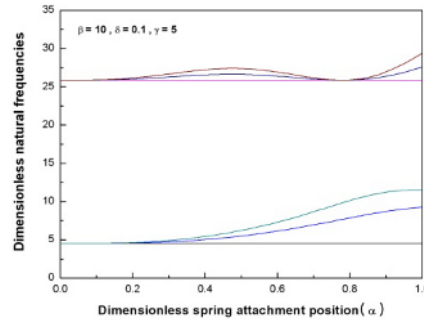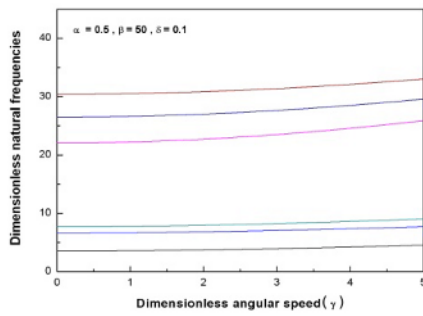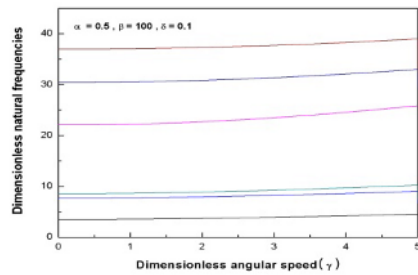Fig. 5. Lowest 8 natural frequencies versus the spring attachment position.

first four mode shapes consists of the first bending modes and the next four mode shapes consist of the second bending modes. Comparing the 2nd and the 3rd modes (or the 6th and the 7th modes) one can see that the two modes are almost identical if one of them rotates about 90 degrees. Therefore, the natural frequencies of the two modes should be almost identical, too.

Fig. 4 shows the lowest eight dimensionless natural frequencies of the 4-beam system for different values of the dimensionless spring attachment position α. The parameters except α employed for the analysis are same as before. As can be shown in the figure, the lowest frequencies in each group remain unchanged while other frequencies increase. The two middle natural frequencies in each group are the same (as discussed in the previous paragraph) so that only three loci for each group can be observed in the figures. As α increases, the gaps between the frequencies increase significantly.

Fig. 5 shows the lowest eight dimensionless natural frequencies of 4-beam system versus the dimensionless spring attachment position α. The parameters employed for the analysis are $\beta = 10$, $\gamma = 5$ and $\delta = 0.1$. As α increases, the natural frequencies vary. An interesting fact one can observe from the figure is that the second group of natural frequencies

increase as α increases initially. However, they decrease after reaching their maximum values and become identical at a specific value of α. The location of α is actually the same as the nodal point of the rotating beam.

Fig. 6 shows the lowest eight dimensionless natural frequencies of the 4-beam system for different values of the dimensionless coupling stiffness β.

The parameters are employed the analysis are $\alpha = 0.5$ and $\delta = 0.1$. As shown in the figures, the

(a) $\beta = 50$

(b) $\beta = 100$

Fig. 6. Lowest 8 natural frequencies versus the angular speed for different values of β.
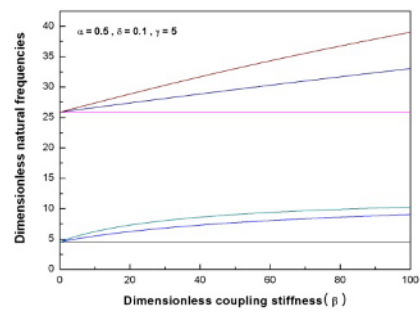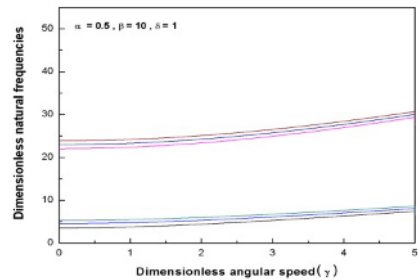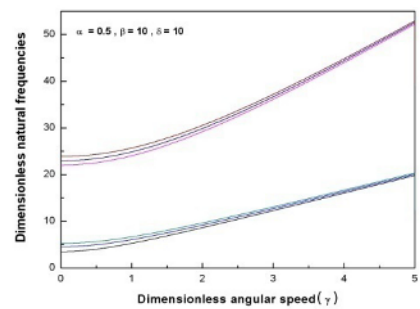

Fig. 7. Lowest 8 natural frequencies vs. the coupling stiffness.

(a) $\delta = 1$

(b) $\delta = 10$

Fig. 8. Lowest 8 natural frequencies versus the angular speed for different values of δ.

lowest frequencies in each group remain unchanged. It can be observed from the figures that the gaps between the frequencies increase as the coupling stiffness β increase. However, the gap variation between frequencies in the first group is less affected by β (compared to α).

Fig. 7 shows the lowest eight dimensionless natural frequencies of the 4-beam system versus the dimensionless coupling stiffness β. The parameters employed for the analysis are $\alpha = 0.5$, $\gamma = 5$ and $\delta = 0.1$. As shown in the figures, the natural frequencies (except the lowest ones in each group) increase monotonically as the coupling stiffness increases. The lowest natural frequencies remain unchanged.

Fig. 8 shows the lowest eight dimensionless natural frequencies of the 4-beam system for different value of the dimensionless hub radius ratio. The parameters employed for the analysis are $\alpha = 0.5$ and $\beta = 10$. As can be shown in the figure, the slopes of the natural frequencies become stiffer as the hub radius ratio δ increases. This can be easily understood since the larger hub radius results in larger centrifugal force, which results in larger motion-induced stiffness for the system.

Fig. 9 shows the lowest eight dimensionless natural frequencies of 4-beam system versus the dimensionless hub radius ratio δ. The parameters employed for the analysis are $\alpha = 0.5$, $\beta = 10$, and $\gamma = 5$. The figure shows that the natural frequencies increase approximately in proportion to the square root of the hub radius ratio. Since the stiffness of the motion induced stiffness is proportional to the hub radius, the natural frequency should be approximately in proportional to the hub radius.

Fig. 10 shows two groups of dimensionless natural frequencies for 6-beam system and 8-beam system. The parameters employed for the analysis are $\alpha = 0.5$,
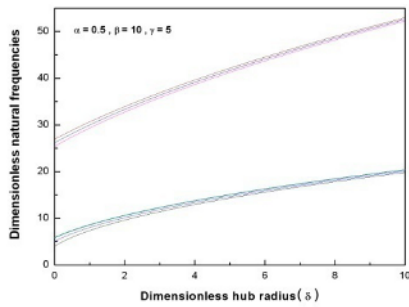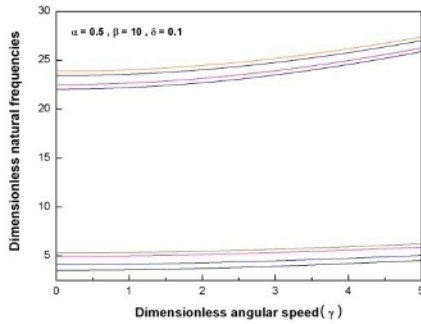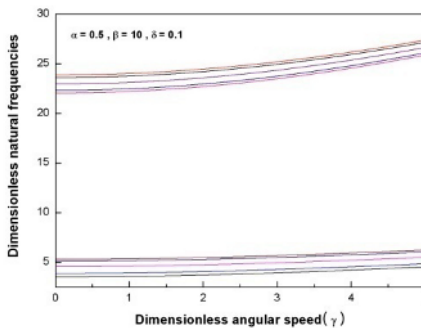
Fig. 9. Lowest 8 natural frequencies vs. the hub radius.

(a) number of blades = 6

(b) number of blades = 8

Fig. 10. Effect of the number of blades on the natural frequencies.

4. Conclusions

A dynamic modeling method to derive the equations of motion of a rotating multi-blade system is presented in this paper. The modeling method employs a set of hybrid deformation variables with which the motion-induced stiffness variation effect can be included in the equations of motion. The equations of motion are transformed into a dimensionless form in which dimensionless parameters related to the angular speed, the coupling stiffness, the location of coupling stiffness and the hub radius are identified. Numerical results show that the natural frequencies increase as the angular speed increases. As the hub radius increases, the increasing slope becomes stiffer. The gap between the frequency loci increases as the coupling stiffness or the location of coupling stiffness increases. Finally, the gap between the lowest natural frequency and the highest natural frequency is rarely affected by the number of blades. Therefore, as the number of blades increases, the gap between any two frequency loci decreases.

References

[1] R. Southwell and F. Gough, The free transverse vibration of airscrew blades, *British A. R. C. Reports and Memoranda* 766 (1921).

[2] M. Schilhansl, Bending frequency of a rotating cantilever beam, *J. of Appl. Mech. Trans. Am. Soc. Mech. Engrs* 25 (1958) 28-30.

[3] A. Leissa, Vibration aspects of rotating turbomachinery blades, *Applied Mechanics Reviews* 34 (1981) 629-635.

[4] J. Rao, Turbomachine blade vibration, *Shock Vibration Digest* 19 (1987) 3-10.

[5] T. Kane, R. Ryan, and A. Banerjee, Dynamics of a cantilever beam attached to a moving base, *Journal of Guidance, Control, and Dynamics* 10(2) (1987) 139-151.

[6] H. Yoo, R. Ryan, and R. Scott, Dynamics of flexible beams undergoing overall motions, *Journal of Sound and vibration* 181 (1995) 261-278.

[7] H. Yoo and S. Shin, Vibration analysis of rotating cantilever beams, *Journal of Sound and Vibration* 212 (1998) 807-828.

[8] M. Singh and D. Schiffer, Vibrational characteristics of packeted bladed discs, *ASME Paper* No. 82-DET-137 (1982).

[9] M. Singh, J. Vargo, D. Schiffer and J. Dello, Safe diagram – A design reliability tool for turbine blad-

$\beta = 10$ and $\delta = 0.1$. It seems that there exist only eight natural frequency loci in Fig. 10(a) and ten natural frequency loci in Fig. 10(b). However, every locus in the middle of each group contains two sets of natural frequency information.

As shown in the figure, the gap between the lowest natural frequency and the highest natural frequency is rarely affected by the number of blades. Therefore, the gap between any adjacent two loci decreases as the number of blades increases.

ing, *Proceedings of the Seventeenth Turbomachinery Symposium* Texas A&M Universiy (1988) 93-101.

[10] T. Kane and D. Levinson*, Dynamics: Theory and Applications*, McGraw-Hill Book Co., New York, N. Y (1985).

Ha Seong Lim graduated from Department of Mechanical Engineering at Hanyang University in 2006 and received his Master's degree in 2008. He is currently a technical engineer in STX Offshore & Shipbuilding Company, Seoul, Korea..

Hong Hee Yoo graduated from the Department of Mechanical Design and Production Engineering at Seoul National University in 1980 and received his Master's degree from the same department in 1982. He received his Ph.D. degree in 1989 from the Department of Mechanical Engineering and Applied Mechanics at the University of Michigan at Ann Arbor, U.S.A. He is currently a professor in the School of Mechanical Engineering in Hanyang University, Seoul, Korea.